

# Multimessenger observations of counterparts to IceCube-190331A

Felicia Krauß,<sup>1\*</sup> Emily Calamari,<sup>2†</sup> Azadeh Keivani,<sup>3,4‡</sup> Alexis Coleiro,<sup>5</sup>  
 Phil A. Evans,<sup>6</sup> Derek B. Fox,<sup>1,7,8</sup> Jamie A. Kennea,<sup>1</sup> Peter Mészáros,<sup>1,7,8</sup>  
 Kohta Murase,<sup>7</sup> Thomas D. Russell,<sup>9</sup> Marcos Santander,<sup>10</sup> and Aaron Tohuvavohu<sup>1,11</sup>

<sup>1</sup>Department of Astronomy & Astrophysics, Pennsylvania State University, University Park, PA 16802, USA

<sup>2</sup>Department of Physics, Barnard College, Columbia University, New York, NY 10027, USA

<sup>3</sup>Department of Physics, Columbia University, New York, NY 10027, USA

<sup>4</sup>Columbia Astrophysics Laboratory, Columbia University, New York, NY 10027, USA

<sup>5</sup>APC, Univ Paris Diderot, CNRS/IN2P3, CEA/Irfu, Obs de Paris, Sorbonne Paris Cité, France

<sup>6</sup>Department of Physics & Astronomy, University of Leicester, Leicester, LE1 7RH, UK

<sup>7</sup>Center for Particle & Gravitational Astrophysics, Institute for Gravitation and the Cosmos, Pennsylvania State University, University Park, PA 16802, USA

<sup>8</sup>Center for Theoretical & Observational Cosmology, Institute for Gravitation and the Cosmos, Pennsylvania State University, University Park, PA 16802, USA

<sup>9</sup>Anton Pannekoek Institute for Astronomy, University of Amsterdam, Science Park 904, 1098XH Amsterdam, the Netherlands

<sup>10</sup>Department of Physics and Astronomy, University of Alabama, Tuscaloosa, AL 35487, USA

<sup>11</sup>University of Toronto, Toronto, Canada

Accepted 2020 July 17. Received 2020 July 3; in original form 2020 May 22

## ABSTRACT

High-energy neutrinos are a promising tool for identifying astrophysical sources of high and ultra-high energy cosmic rays (UHECR). Prospects of detecting neutrinos at high energies ( $\gtrsim$  TeV) from blazars have been boosted after the recent association of IceCube-170922A and TXS 0506+056. We investigate the high-energy neutrino, IceCube-190331A, a high-energy starting event (HESE) with a high likelihood of being astrophysical in origin. We initiated a *Swift*/XRT and UVOT tiling mosaic of the neutrino localisation, and followed up with ATCA radio observations, compiling a multiwavelength SED for the most likely source of origin. *NuSTAR* observations of the neutrino location and a nearby X-ray source were also performed. We find two promising counterpart in the 90% confidence localisation region and identify the brightest as the most likely counterpart. However, no *Fermi*/LAT  $\gamma$ -ray source and no prompt *Swift*/BAT source is consistent with the neutrino event. At this point it is unclear whether any of the counterparts produced IceCube-190331A. We note that the Helix Nebula is also consistent with the position of the neutrino event, and we calculate that associated particle acceleration processes cannot produce the required energies to generate a high-energy HESE neutrino.

**Key words:** neutrinos — galaxies: active — BL Lacertae objects: general — quasars: general — galaxies: jets

## 1 INTRODUCTION

Cosmic rays arriving at Earth have been detected up to the extreme energies of  $10^{21}$  eV since more than a century ago – yet their origin remains elusive (e.g., Norman et al. 1995). A promising tool for identifying the astrophysical sources

of high and ultra-high energy cosmic rays are high-energy neutrinos as they are not deflected in interstellar and intergalactic magnetic fields. Consistent with these expectations, a diffuse extraterrestrial flux of high-energy neutrinos has been observed by the IceCube neutrino observatory over more than a decade of observation (Aartsen et al. 2013; IceCube Collaboration 2014; Haack & Wiebusch 2017). Localisation uncertainties mean that the nature of these neutrinos is still unknown.

Blazars and other types of AGN have been predicted to

\* E-mail: Felicia.Krauss@psu.edu

† ecalamari@gradcenter.cuny.edu

‡ azadeh.keivani@columbia.edu

produce neutrinos in jets (Biermann & Strittmatter 1987; Mannheim et al. 1991; Mannheim 1993, 1995) and/or in their cores (Eichler 1979; Berezhinskii & Ginzburg 1981; Begelman et al. 1990; Stecker et al. 1991; Stecker 2013). TeV and PeV neutrinos are expected from flat-spectrum radio quasars, while BL Lacs are expected to produce neutrinos at EeV energies. Recently, progress has also been made in explaining neutrinos from BL Lac objects (Murase et al. 2014; Dermer et al. 2014; Tavecchio & Ghisellini 2015). We have shown that blazars can calorimetrically explain IceCube neutrinos (Krauß et al. 2014), low-significance coincidence between a blazar outburst and an astrophysical neutrino, IC 35 (and PKS 1424–418; Kadler et al. 2016). To date, the neutrino candidate, IceCube-170922A has only been the second  $\gtrsim 3\sigma$  association of neutrino emission to an astronomical source (SN 1987A; blazar TXS 0506+056; IceCube Collaboration, Fermi-LAT Collaboration et al. 2018; Keivani et al. 2018). However, it has also been shown that for realistic neutrino spectra, blazars can account for all IceCube high-energy neutrinos (Krauß et al. 2018); this is in disagreement with the 30% limit on the contribution of blazars found by Aartsen et al. (2017b) for all IceCube neutrinos. More stringent limits of 5–15% have been placed by Hooper et al. (2019); Yuan et al. (2020), which would still be consistent with a significant contribution of AGN, including blazars, to the PeV neutrinos (Murase & Waxman 2016). It is possible that non-blazar AGN produce the entire or a large fraction of the astrophysical neutrino flux seen by IceCube (Hooper et al. 2019). Some authors have argued for a combination of BL Lac and pulsar wind nebula as the origin of the IceCube neutrinos (Padovani & Resconi 2014).

While blazars and other active galactic nuclei (AGN) are excellent candidates for accelerating cosmic rays to ultra-high energies, significant contributions from other types of sources are not yet ruled out. Suggested populations include starburst galaxies (Murase et al. 2013; Senno et al. 2015; Bechtol et al. 2017), and (choked) GRBs (Murase & Ioka 2013; Senno et al. 2016; Tamborra & Ando 2016; Aartsen et al. 2017c).

IceCube and the Astrophysical Multimessenger Observatory Network (AMON)<sup>1</sup> started a real-time program in 2016 (Aartsen et al. 2017a) to identify and localise high-energy neutrinos in order to distribute them to follow-up observatories. Since 2019 IceCube provides these alerts at “bronze”, “silver” and “gold” levels. There have been 17 such alerts as of February 2020 (10 “bronze” alerts and 7 “gold” alerts), several of which resulted in extensive multimessenger campaigns to observe the location of the neutrino candidate in different wavelengths/messengers. IceCube-170922A has so far been the only event with a  $\gtrsim 3\sigma$  source identification (IceCube Collaboration, Fermi-LAT Collaboration et al. 2018).

On March 31, 2019, the IceCube Neutrino Observatory identified a high energy neutrino candidate (labelled IceCube-190331A), likely produced by a muon neutrino. This event was publicly distributed through the gamma-ray coordinates network (GCN; Barthelmy et al. 1995) within 34 seconds (GCN/AMON NOTICE IceCube-190331A 2017). A subsequent search by Fermi/LAT determined there were no

known  $\gamma$ -ray sources within the 90% IceCube-190331A localisation error (Buson & Garrappa 2019). Given the event direction, this paper seeks to investigate a possible origin for this high-energy neutrino candidate by conducting follow-up observations of known sources within the uncertainty region.

We report the multiwavelength observations (radio, optical, UV, X-ray) of possible counterparts detected by Swift/XRT during follow-up observations of the IceCube-190331A high-energy neutrino candidate (Sec. 2) and discuss possible associations with the IceCube event (Sec. 3).

Throughout the paper we use the standard cosmological model with  $\Omega_m = 0.3$ ,  $\Lambda = 0.7$ ,  $H_0 = 70 \text{ km s}^{-1} \text{ Mpc}^{-1}$  (Berlinger et al. 2012).

## 2 OBSERVATIONS

In this section, we review the detection of the IceCube-190331A neutrino event, and present observations and data analysis of electromagnetic follow-up observations from Swift (X-ray, ultraviolet/optical,  $\gamma$ -ray), ATCA (radio), X-shooter (ultraviolet, optical, near-infrared), and NuSTAR (X-ray).

### 2.1 IceCube Detection

On March 31, 2019, the IceCube Neutrino Observatory identified a high-energy neutrino candidate through its High Energy Starting Event (HESE) stream. This event had a high probability of being produced by a muon neutrino of astrophysical origin with a deposited charge of about 198736.44 photoelectrons in the detector (GCN/AMON NOTICE IceCube-190331A 2017). This event was recorded as having one of the highest deposited energies ever seen, making it a promising astrophysical neutrino candidate (Kopper & Blaufuss 2017). After conducting a ground-based analysis using offline reconstruction algorithms, IceCube was able to report an event direction at RA=337°68<sup>+0.23</sup><sub>-0.34</sub>, Dec=-20°70<sup>+0.30</sup><sub>-0.48</sub> (J2000; 90% containment ellipse; Kopper & Blaufuss 2017; Ice Cube Collaboration 2019). Subsequently, an additional search for track-like muon neutrino events arriving from the direction of IceCube-190331A was performed by IceCube for two days after the initial event time, as well as a search to include the previous month of data. No additional track-like events were found within the 90% spatial containment region in either search (Icecube Collaboration 2019).

Several multiwavelength follow-up observations were conducted in order to find potential EM counterparts to the very high energy neutrino candidate. Although these searches did not find any high-confidence EM counterpart (Buson & Garrappa 2019), we discuss two possible counterparts below (see Sect. 3).

### 2.2 Swift/BAT prompt observations

At the time of arrival of IceCube-190331A (T0), the neutrino localisation region was serendipitously located near the highest sensitivity location of the coded field-of-view (89% partial coding fraction) of the Swift Burst Alert Telescope (BAT; Barthelmy et al. 2005). This allows us to set

<sup>1</sup> see <https://www.amon.psu.edu/> for details.

**Table 1.** Source found by *Swift*/XRT with their best fit centroid position, as well as source significance. Source #4 is at the lowest significance.

Sources ID	R.A. [J2000]	Dec. [J2000]	Significance $\sigma$
1	337.3551	-20.31325	5.56
2	337.5285	-21.0994	5.06
3	338.0251	-21.0493	4.52
4	338.0184	-21.1199	4.16

sensitive upper limits on the existence of a prompt gamma-ray transient coincident with (or directly preceding or succeeding) the high-energy neutrino emission. We perform a blind search on the BAT raw light curves with time-bins of 64 ms, 1 s, and 1.6 s. We find no evidence for any short or long GRB-like emission within  $T_0 \pm 500$  s of the neutrino arrival time, and set a conservative  $5\sigma$  upper limit for any short GRB of  $\sim 1.5 \times 10^{-7}$  erg s $^{-1}$  cm $^{-2}$ .

We also performed a search for longer time-scale emission, on a survey image produced by the BAT from  $T_0-580$ s to  $T_0+660$ s. We find no new or uncatalogued hard X-ray sources within the neutrino localisation region, and set a  $3\sigma$  flux upper limit of  $\sim 15$  mCrab assuming a powerlaw spectral index of  $\Gamma = 2.15$ .

### 2.3 *Swift*/XRT observations

IceCube-190331A triggered the Neil Gehrels *Swift* Observatory in automated fashion via the AMON cyberinfrastructure (Ayala Solares et al. 2019), however prompt observation of the neutrino localisation was not possible with *Swift* as it was initially within the satellite’s Sun avoidance region. *Swift* observations of the IceCube-190331A field began on April 9, 2019, nine days after the event. *Swift* was able to observe a region of approximately 33’ radius centred on the event direction of RA=337°68, Dec=-20°70 (J2000), using an on-board 7-point tiling pattern (Keivani et al. 2019). During this initial observation, *Swift*/XRT collected approximately 800 seconds of data per tile for a total of  $\sim 5540$  seconds the morning of April 9 and was able to detect four X-ray sources (see Table 1) with the new XRT detection system (Evans et al. 2019). The highest significance (source #1) found during these observations is catalogued at RA=337°35513, Dec=-20°31324 (J2000; 90 % containment region), matching the known X-ray source 1WGA J2229.4–2018 from ROSAT/WGACAT catalogue (15.37’’ distance; White et al. 1994). Another source, 5.3’’ away from X-ray source # 1 is listed in the Milliquas catalogue (Flesch 2017) as the likely AGN WISEA J222925.59–201846.0 and is consistent with the J=16.74 mag 2MASS source (2MASS J22292559–2018462, see Fig. 1; Skrutskie et al. 2006; Keivani et al. 2019). WISEA J222925.59–201846.0 is not listed in the most recent ALLWISE catalogue, so the WISEA detection might not be real (Wright et al. 2010).

Although it seems that the sources (WISEA J222925.59–201846.0 /2MASS J22292559–20184 and 1WGA J2229.4–2018) are the same, it is possible that neither 1WGA J2229.4–2018 nor WISEA J222925.59–201846.0 are real source detections, but rather background fluctuations, given their low detection

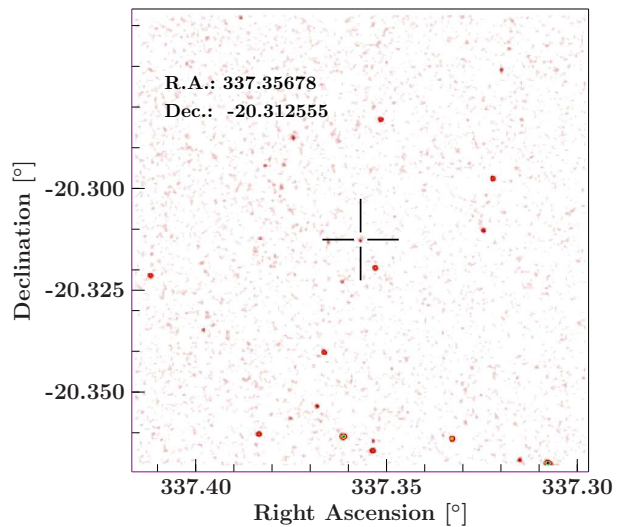


**Figure 1.** K-Band 2MASS image of the region surrounding 2MASS J22292559–2018462.

significance and distance from the 2MASS J22292559–20184 coordinates.

*Swift*/XRT performed a further observation centred on the location of source #1. The X-ray analysis following the observation period 58582.323 - 58582.471 MJD focused on data from the most significant sources and did not consider the lower-significance X-ray sources. The data used in analysis were from *Swift*/XRT observations of the position of 1WGA J2229.4–2018 (source #1) on April 9, 2019 and April 16, 2019. The newest calibration was applied using the xrt-pipeline to the raw data using HEASoft (V. 6.26). Spectra were extracted from the reprocessed image using a source region with 54.218’’ radius and an annulus for the background region of 82.506 and 235.721’’ using XSELECT (V. 2.4). Due to the low count rate, data were binned to a signal-to-noise-ratio (SNR) of 1 in the *Interactive Spectral Interpretation System* (ISIS; V. 1.6.2-44; Houck & Denicola 2000). Due to the low SNR we use Cash statistics to find a best fit (Cash 1979). The data were fit with an absorbed power law with a convolution model to calculate the flux. For the absorption model we use tbnew<sup>2</sup> with the vern cross-sections (Verner et al. 1996) and the wilm abundances (Wilms et al. 2000). The hydrogen equivalent absorption column density was frozen to a value of  $3.55 \times 10^{20}$  cm $^{-2}$  (HI4PI Collaboration et al. 2016a).

The photon indices for the observations on April 9 and April 16 were found to be  $\Gamma_1 = 2.4^{+4.3}_{-1.4}$  and  $\Gamma_2 = 2.4^{+1.6}_{-0.8}$ , respectively, with corresponding flux values of  $(1.1^{+0.7}_{-0.9}) \times 10^{-13}$  and  $(1.6^{+1.0}_{-0.9}) \times 10^{-14}$  erg s $^{-1}$  cm $^{-2}$ , indicating a possible change in flux. Uncertainties for both the photon index and flux were calculated at the 90% confidence level. Both observations are combined in the SED and shown with a signal-to-noise ratio binning of 2 (see Fig. 2).

<sup>2</sup> online at: <http://pulsar.sternwarte.uni-erlangen.de/wilms/research/tbabs/>

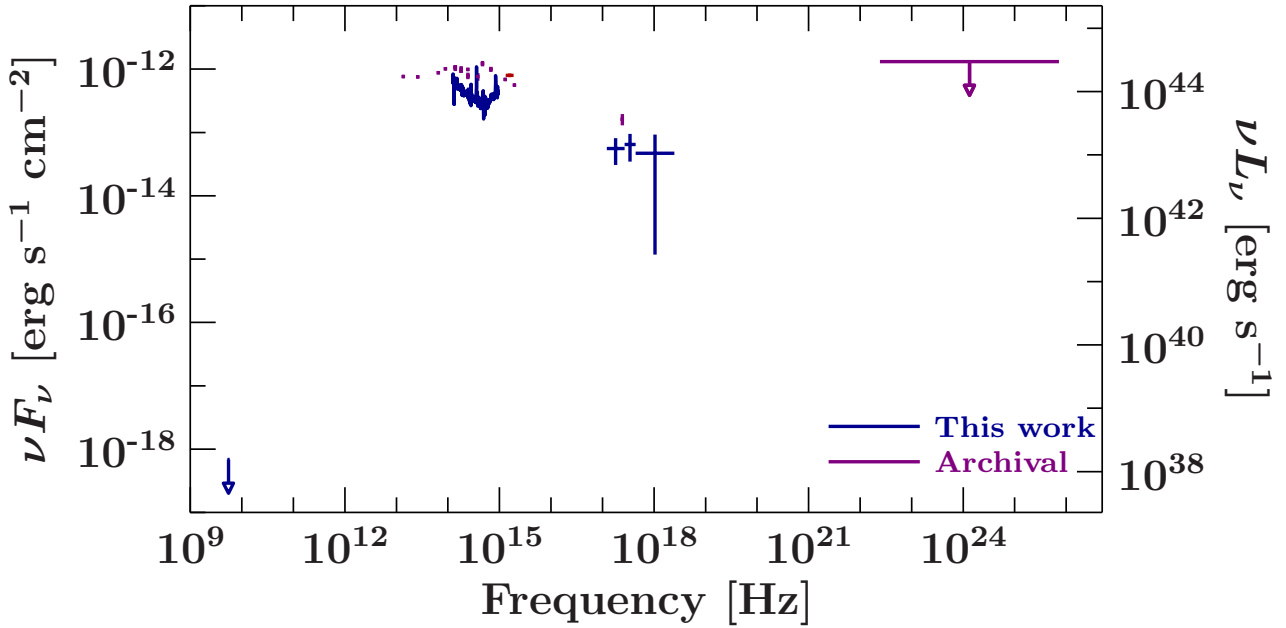


**Figure 2.** Multiwavelength SED of source #1, including our ATCA, X-Shooter, and *Swift*/XRT data. Archival data is shown in purple.

#### 2.4 *Swift*/UVOT follow-up observations

The *Swift*/UltraViolet-Optical Telescope (UVOT) (Roming et al. 2005) also participated in both the tiling and targeted follow-up in response to IceCube-190331A. Only source #2 was within the field of view of the initial tiled UVOT observations (see Fig. 3). An additional follow-up observation on April 16 provided a UVOT image for source #1 for a cleaned exposure time of 2829s in the *uvw2* filter. UVOT images in one observations were summed using *uvotimsum*. Source counts were extracted using *uvot2pha* with a 5'' region at an updated source position of RA=337°5298451, Dec=-21°09967127 and annulus for the background region of 13 and 26'', centred on the source position while ensuring no contamination from background sources. Source #1 was extracted with regions of the same size, centred on RA=337°3566258, Dec=-20°3127867. Additionally, *uvw2* images detected WISEA J222925.59-2201846.0 at an AB magnitude of  $19.64^{+0.08(\text{stat})}_{-0.03(\text{sys})}$ . No flux variability or changes were detected in the four observations.

We performed a search for uncatalogued sources in the UVOT *u*-band with observations taken during the 7-point tiling follow-up. No new or uncatalogued sources were found down to an average  $5\sigma$  upper limit of  $u=20.3$  mag AB.

#### 2.5 X-Shooter Observation

Medium-resolution spectroscopy of 1WGA J2229.4-2018 was obtained with the X-shooter spectrograph (Vernet et al. 2011) of the Very Large Telescope (VLT) UT2 at the ESO Paranal Observatory on 2019 April 26. The three arms of X-shooter, (UV: UVB, optical: VIS and near-infrared: NIR) were used with slit widths of 1''0, 0''9, and 0''9, respectively. These data provide quasi-simultaneous 300–2400 nm spectral coverage with average spectral resolutions  $\lambda/\Delta\lambda$  of 5400, 8900, and 5600, respectively, in each arm. Observing conditions were intermediate, with a clear sky, a seeing of  $\sim 1''5$ ,

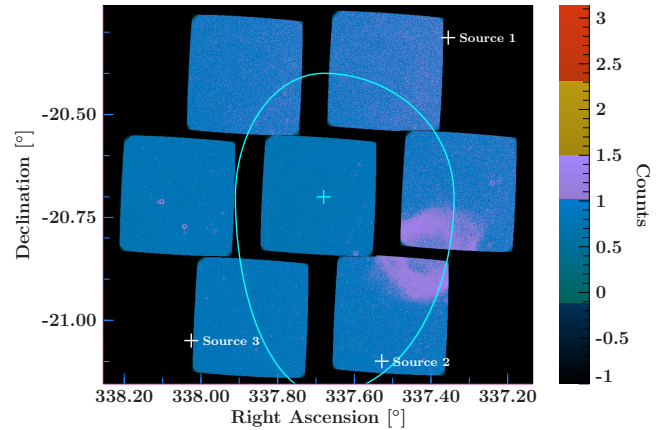


**Figure 3.** *Swift*/UVOT mosaic follow-up of the localisation region of IceCube-190331A. The Helix nebula, NGC 7293, is clearly visible in the west. It is not detected at X-ray energies. The cyan cross shows the best fit position of the neutrino event. The 90% containment region is given in cyan, following the values from Ice Cube Collaboration (2019).

and an airmass of 1.7. Individual exposure times are 445 s, 352 s, and 200 s for the UVB, VIS, and NIR arms, respectively, which lead to a total integration times of 3560 s, 2816 s, and 3200 s. Standard ABBA nodding observing mode was used to allow for an effective background subtraction. Data were reduced using the ESO X-shooter pipeline (Goldoni et al. 2006; Modigliani et al. 2010) (v.2.9.3), producing a background-subtracted, wavelength-calibrated spectrum. The extracted 1D spectrum was flux calibrated with the X-shooter pipeline using a response function produced by observing the white dwarf standard LTT 3218 (R.A. 08h 41m 32s.43, Dec. -32° 56' 32.9'', J2000) during the same night. The spectrum was corrected from telluric absorption lines



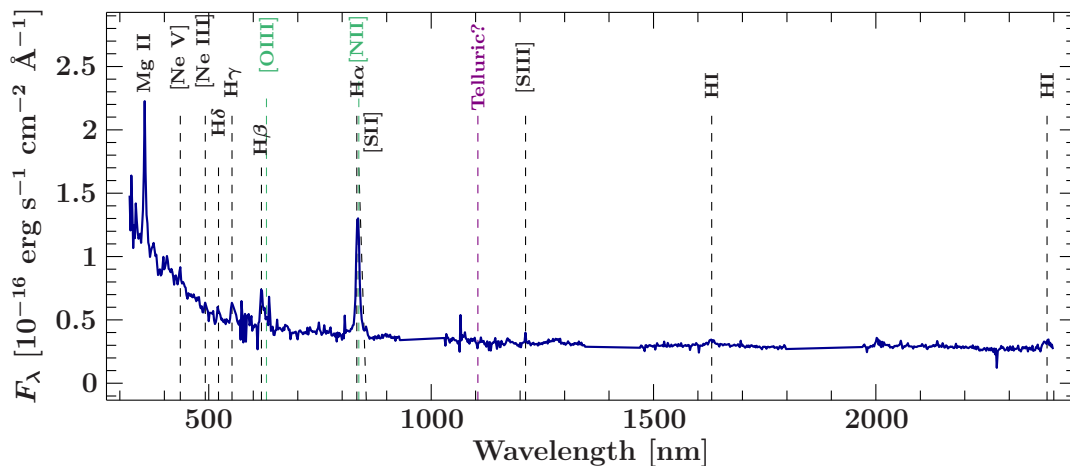


Figure 4. X-Shooter spectrum of 1WGA J2229.4-2018.

using the Molecfit package (Smette, A. et al. 2015), and the flux was dereddened using (Cardelli et al. 1989) with  $A_V=0.1358$  mag and  $R_V=3.1$ .

The reduced 1D spectrum is shown in Figure 4. It is dominated by strong MgII (279.8 nm - rest frame) and Balmer  $H\alpha$ ,  $\beta$ ,  $\gamma$ ,  $\delta$  emission lines that allow to derive a source redshift of  $z = 0.27$ . Forbidden lines of [O III] (495.9 nm; 500.7 nm), [Ne V] (342.6 nm), [Ne III] (386.9 nm), [N II] (658.3 nm), [S II] (671.6 nm) and [S III] (953.1 nm) are also present. While HI and MgII broad allowed emission lines presumably form within the accretion disk or close to it, narrow forbidden lines of neon, oxygen and sulfur are supposed to come from lower density regions further away from the supermassive black hole. The X-shooter rest-frame spectrum of 1WGA J2229.4-2018 matches with the optical spectrum of a Seyfert 1.2 AGN with [O III] lines weaker than the  $H\alpha$  one. The  $\nu F_\nu$  optical/near-infrared spectral energy distribution of 1WGA J2229.4-2018 displays a deep trough around  $10^{14.8}$  Hz which probably indicates the transition between the dusty torus and the disk contributions strengthening the classification of the source as a Seyfert 1.2 AGN.

Fig. 4 shows our spectrum of 1WGA J2229.4-2018. We derive a source redshift of  $z = 0.27$  using the emission lines of Mg II, Ne V,  $H\beta$ , and  $H\alpha$  and we use this number to calculate the absolute luminosity of the source and its SED. Based on the optical spectrum the source can be identified as Seyfert type I AGN.

## 2.6 ATCA Observation

Following the detection of the neutrino candidate IceCube-190331A, we requested radio observations with the Australia Telescope Compact Array (ATCA; under project code CX433) targeting the four X-ray sources found by *Swift*/*XRT* within the neutrino location error region. The ATCA observations were carried out on 2019 April 21 and 22. On the first night ATCA observed X-ray sources 1, 3, and 4, while on the second night it targeted X-ray sources 1 and 2. The observations were recorded simultaneously at central frequencies of 5.5 and 9 GHz, with 2 GHz of bandwidth at each frequency. We used PKS 1934-638 for bandpass and flux calibration, while the nearby source J2203-188 was used

Table 2. The ATCA flux upper limits and the corresponding coordinates. The ID gives the *Swift* /XRT source ID. Right ascension and declination give the centre of the region that was used for determining the upper limit. The coordinates for source # 2 are offset due to flux from a nearby source. The uncertainties on the right ascension and declination are  $0.2''$  and  $0.5''$ , respectively.

ID	RA [J2000]	Dec [J2000]	Flux UL [ $\mu$ Jy/beam]
1	337.35513	-20.31324	12.36
2	337.53187	-21.10525	27.62
3	338.02441	-21.04247	46.72

for phase calibration. The data were edited, calibrated, and imaged following standard procedures within the Common Astronomy Software Application (CASA, version 5.1.0; McMullin et al. 2007). Imaging was done using a Briggs robust parameter of 2 to maximise sensitivity. Since X-ray source #1 was observed on both days, the two observations were combined to maximise sensitivity.

No radio counterpart was detected at any of the X-ray source positions. Upper limits were determined by stacking the 5.5 and 9 GHz data and taking three times the measured rms over the source position. They were extracted from regions of  $30''$  centred on the source positions. The flux densities of nearby sources are reported as the peak pixel flux density. To determine the position of these nearby radio sources, we fit for point sources in the image plane. The resulting values are given in Table 2. ATCA finds no source consistent with the X-ray detection of source 1 (see Fig. 5); it only finds a source offset from the X-ray position. Source 2 shows a possible ATCA counterpart with a faint jet feature in the stacked image (Fig. 6). Source 3 shows a very faint source south of the X-ray coordinates, which is likely unrelated to the X-ray source. A brighter AGN is visible, east of the coordinates.

The derived flux upper limit for source #1 is shown in the multiwavelength SED (Fig. 2).

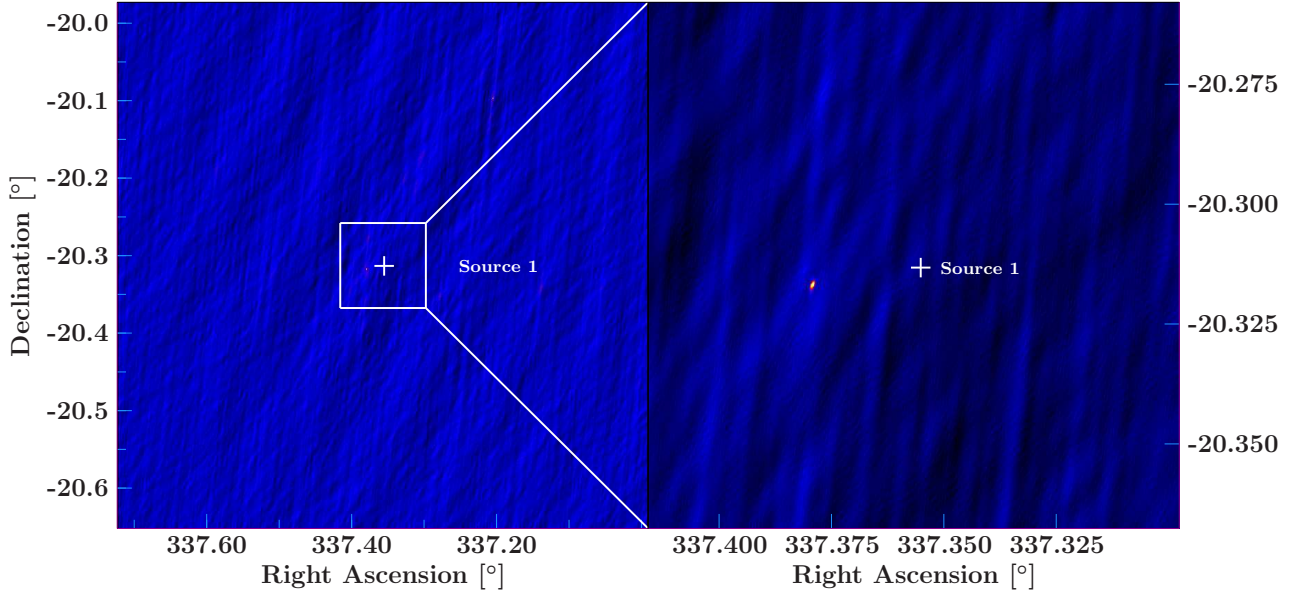


**Figure 5.** Stacked ATCA image near source 1. No radio source is detected that corresponds to the X-ray source. A radio source - likely a previously unknown AGN - is visible to the east of Source 1, at a distance of  $2.52'$ .

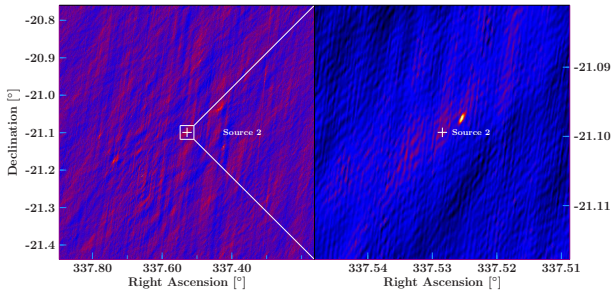


**Figure 6.** Stacked ATCA image near source #2, a radio source is visible to the north-west. It is unclear whether it is connected to the X-ray detection.

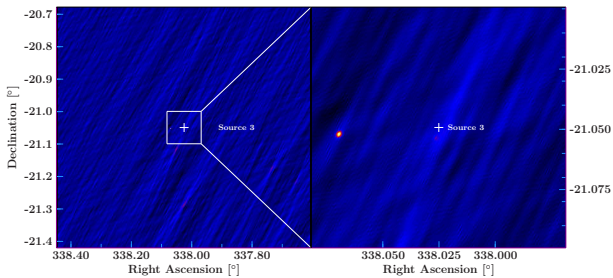


**Figure 7.** Stacked ATCA image near source 3. No bright counterparts is visible.

## 2.7 NuSTAR observations

Following the detection of IceCube-190331A we requested target of opportunity observations using the NuSTAR X-ray satellite (Harrison et al. 2013) to search for hard X-ray sources coincident with the neutrino event.

Two observations were performed: the first (ObsID 90502615001, started on 2019 April 2 UT) targeting the best-fit neutrino position, and the second (ObsID

90502616001, 2019 April 3) on the nearby *Fermi*/LAT source 4FGL J2232.6-2023, associated with the hard X-ray source 1RXS J223249.5-202232, a BL Lac object at a redshift of 0.386 (Jiménez-Bailón et al. 2012). A sky map containing data from both exposures plus their relative locations with respect to the neutrino event and *Swift* pointings is shown in Fig. 8.

Both focal plane modules (FPMs A and B) were used to collect data, which were then processed using version 1.9.2 of the NuSTARDAS software included in HEASOFT v6.27.2 and analysed using XSPEC v12.11.0.

### 2.7.1 Observation of the IceCube-190331A position

A total exposure of 5.5 ks per FPM was collected at the IceCube-190331A position. The observations did not reveal any new X-ray sources and therefore we derive a flux upper limit at the best-fit neutrino location. The observations from both FPMs were first combined and a  $3\sigma$  count rate upper limit was calculated using the `uplimit` routine in XIMAGE which implements the Bayesian approach of Kraft et al. (1991). This upper limit was calculated for a circular region with a  $30''$  radius centred at the best-fit neutrino location, but given the homogeneity of the field we expect it to be illustrative of the entire NuSTAR exposure. The count rate upper limit is 4.66 counts / ks, which corresponds to a flux upper limit of  $1.604 \times 10^{-13}$  erg cm $^{-2}$  s $^{-1}$  in the 3-10 keV range as calculated using the WebPIMMS tool<sup>3</sup> for a photon index of  $\Gamma = 2.0$ .

<sup>3</sup> <https://heasarc.gsfc.nasa.gov/cgi-bin/Tools/w3pimms/w3pimms.pl>

### 2.7.2 Observation of 1RXS J223249.5-202232

An exposure of 5.1 ks per FPM was obtained targeting 1RXS J223249.5-202232. The spectral data from both FPMs were combined using the `addspec` routine following the procedure recommended by the *NuSTAR* science team and then grouped requiring at least 30 counts in each spectral bin. The resulting spectrum covers the 3–15 keV range with good statistics after bad channels are excluded. The spectrum was then fit with an absorbed power-law model (`phabs` × `powerlaw`, PL hereafter) where the absorption was kept fixed at the Galactic HI column contribution of  $3.33 \times 10^{20} \text{ cm}^{-2}$  obtained from [HI4PI Collaboration et al. \(2016b\)](#)<sup>4</sup>.

The best-fit PL parameters (for the form  $N(E) = N_0 E^{-\Gamma}$ ) were a flux normalisation  $N_0 = (1.88 \pm 0.76) \times 10^{-3} \text{ cm}^{-2} \text{ keV}^{-1} \text{ s}^{-1}$ , at a normalisation energy of 1 keV, and a photon index  $\Gamma = 2.87 \pm 0.24$ . These parameters yield a good fit, with a  $\chi^2/\text{dof} = 6.33/7$  ( $p$ -value of 0.502). A second fit was attempted to test for intrinsic absorption at the source using the `zphabs` model and the source redshift but this failed to constrain the intrinsic absorption given the limited statistics of the data set.

Using the best-fit model we calculate a flux of  $F = (1.39^{+0.09}_{-0.27}) \times 10^{-12} \text{ erg cm}^{-2} \text{ s}^{-1}$  in the 2–10 keV range. This flux is significantly lower and has a softer photon index than the values reported by [Jiménez-Bailón et al. \(2012\)](#) based on hard-band *XMM-Newton* EPIC observations obtained in 2008 in the same energy range ( $F_{\text{XMM}} = (5.05 \pm 0.04) \times 10^{-12} \text{ erg cm}^{-2}$  and  $\Gamma_{\text{XMM}} = 2.06 \pm 0.03$ ).

### 2.7.3 Summary of NuSTAR results

No new sources were identified in the *NuSTAR* observations near the best-fit neutrino position. Similarly, the known source 1RXS J223249.5-202232 was observed in a low flux state, and no evidence of gamma-ray activity is visible in the online *Fermi* All Sky Variability Analysis (FAVA)<sup>5</sup>, nor was reported at the time of the neutrino alert detection<sup>6</sup>.

We therefore claim no connection between this source and the observation of the IceCube-190331A event. The *NuSTAR* pointings do not cover the new *Swift* sources so no constraints can be derived on their hard X-ray fluxes from these observations.

## 2.8 Helix Nebula

We note that the planetary nebula NGC 7293, more commonly known as the Helix Nebula, is detected on the western side of the UVOT mosaic, within neutrino localisation area. The expected particle energies in a planetary nebula, however, are too low to explain a TeV neutrino event. Planetary nebulae can have fast winds up to  $\sim 1100 \text{ km s}^{-1}$  with a mass loss rate of  $\dot{m} \sim 10^{-11} M_{\odot} \text{ year}^{-1}$  ([Huarte-Espinosa et al. 2012](#)). Using the kinetic luminosity of  $L_k = \dot{m} v^2$ , this

yields the following magnetic luminosity ([Blandford 2000](#))

$$L_B = \epsilon_B L_k = 4 \pi r^2 \cdot v \cdot \left( \frac{B^2}{8 \pi} \right) = \frac{1}{2} r^2 \cdot v B^2, \quad (1)$$

with the magnetic energy fraction  $\epsilon_B < 1$ , the magnetic field  $B$  and the radius of the moving wind  $r$ . After solving for  $r \cdot B$  and using the previously calculated kinetic luminosity, we can use it in

$$E < e \cdot r \cdot B \cdot \frac{v}{c}, \quad (2)$$

using the Hillas condition ( $v/c$ ; [Hillas 1984](#)), with the elementary charge  $e$  and the speed of light  $c$ , to yield

$$E < \sqrt{2 \dot{m} v} \quad (3)$$

This yields a maximum particle energy of

$$E < 0.41 \text{ TeV} \quad (4)$$

The peak energy of neutrinos for  $E^2 dN/dE$  for incident protons with single energy injection is about 3–5% of the energy of the proton (e.g., [Waxman & Bahcall 1997](#); [Kelner et al. 2006](#); [Murase et al. 2006](#)). We would therefore not expect neutrinos above  $\sim 10$ – $20 \text{ GeV}$  from the Helix nebula. For this reason, planetary nebulae have not been considered as sources for high-energy IceCube neutrinos.

## 3 RESULTS & DISCUSSION

We found four X-ray sources in the *Swift*/XRT observations. No new sources, or evidence of X-ray activity in a known source, were identified in the *NuSTAR* observations. We perform follow-up observations on all of them, particularly the brightest three sources. We note that only source #2 is strictly within the IceCube 90% confidence uncertainty region.

We performed detailed follow-up observations of Source #1, the a priori most likely counterpart based on source brightness. The data has been gathered and collected in [Fig. 2](#). With no radio detection and no *Fermi*/LAT detection, but a moderate X-ray luminosity ( $L_{2-10 \text{ keV}} = 1.3^{+2.1}_{-0.9} \times 10^{43} \text{ erg s}^{-1}$ ), we conclude that this source is a possible radio-quiet quasar. A X-Shooter optical spectrum confirms that this object is a type 1 Seyfert galaxy. Neutrinos have been predicted from the cores of AGN in the 10–100 TeV energy range ([Murase et al. 2019](#)). The flare contribution may be subdominant while the core contribution can be dominant in the bulk flux ([Murase et al. 2019](#)). This would change the current picture that particle acceleration in AGN jets is the dominant way to produce neutrinos from AGN ([Kadler et al. 2016](#); [IceCube Collaboration, Fermi-LAT Collaboration et al. 2018](#)), and potentially counterindicated by the high observed energy of this neutrino event.

Neither of the other X-ray sources show obvious counterparts in *Fermi*/LAT or in ATCA observations. Radio sources are detected close to source #2 and source #3, but are not obviously counterparts to the XRT detections. As they have no known counterparts and the X-ray spectrum cannot distinguish between relevant models, we cannot speculate on what source type they are. They could be AGN, or Galactic X-ray sources, such as compact binary objects. However, IceCube-190331A was detected at a Galactic latitude of  $-57^\circ 31'$ , which shows that a Galactic origin is unlikely.

<sup>4</sup> <https://heasarc.gsfc.nasa.gov/cgi-bin/Tools/w3nh/w3nh.pl>

<sup>5</sup> <https://fermi.gsfc.nasa.gov/ssc/data/access/lat/FAVA/LightCurve.php?ra=338.1725&dec=-20.3909>

<sup>6</sup> <https://gcn.gsfc.nasa.gov/gcn3/24040.gcn3>



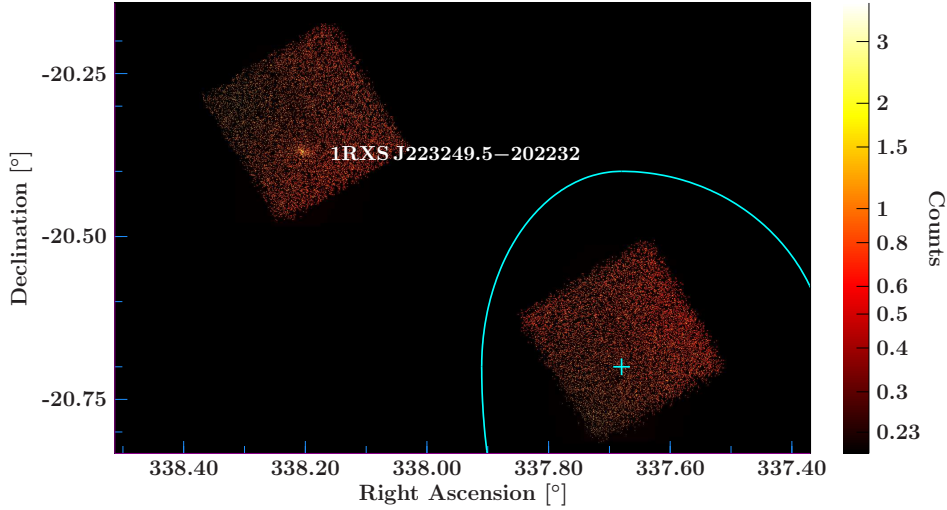


**Figure 8.** *NuSTAR* follow-up observations of the region around IceCube-190331A. The image shows the two *NuSTAR* pointings, with a strong detection of 1RXS J223249.5-202232. The cyan marker and egg-shape indicate the IceCube best fit and 90% containment region for the neutrino event, respectively.

### 3.1 X-ray coincidences

Here, we examine whether observing 1 X-ray sources within and 3 other near the neutrino uncertainty is noteworthy. Given the uncertainties in the right ascension and the declination  $ra_+$ ,  $ra_-$ ,  $dec_+$ , and  $dec_-$ , the equation for the area of the uncertainty region is given by

$$A_{\text{unc}} = \frac{\pi}{2} \cdot \left( \frac{1}{2} \text{dec}_+ \cdot (ra_+ + ra_-) + \frac{1}{2} \text{dec}_- \cdot (ra_+ + ra_-) / 2 \right) \quad (5)$$

which yields  $0.35 \text{ deg}^2$  for IceCube-190331A. Currently, there is no deep full scan of the sky available in the *Swift* X-ray band. A full catalog would give us a precise estimate of the number of X-ray sources expected in this region. As an approximation, we use the ROSAT catalogue as a comparison tool (Boller et al. 2016). The 2RXS catalogue includes 135,118 sources. We select sources above Galactic latitudes of  $\pm 10^\circ$  to give an estimate of the number of extragalactic sources, which yields 117,094 sources. The surface area of the night sky is  $41253 \text{ deg}^2$ . The Galactic plane area that we exclude is given by  $A_{\text{excl}} = 2 \cdot \pi \cdot r \cdot h = 7200^\circ$ , with the radius  $r = 57.3^\circ$  and the height  $h = 20^\circ$ . This yields a total area for the ROSAT sources of  $A_{\text{total}} = 34053 \text{ deg}^2$ . For the IceCube neutrino event, we'd therefore expect  $\sim 1.2$  ROSAT sources within the uncertainty region of  $0.35 \text{ deg}^2$ . While we do find exactly one X-ray source within the uncertainty region, it is not a ROSAT source. This is acceptable considering the low number statistics, and therefore does not point towards an association of the neutrino event and the X-ray source. Given that *Swift*/*XRT* has a wider energy range and more sensitivity, and that the observations were pointed, it is not surprising to find more X-ray sources in the near vicinity.

## 4 CONCLUSIONS

We have performed *Swift*/*XRT*, *Swift*/*UVOT* and *NuSTAR* follow-up observations of the IceCube neutrino alert IceCube-190331A. This event is important as it has a high likelihood of being astrophysical in origin (higher than

IceCube-170922A). We find four X-ray sources in the tiled *Swift*/*XRT* mosaic observations, with two having high detection significance, while no new sources, or activity in a known one, were identified in the *NuSTAR* observations.

The brightest *Swift*/*XRT* source (#1) is consistent with 2MASS J22292559-20184. Due to its known optical counterpart and its X-ray brightness it seemed to be the most likely source of neutrinos. A high X-ray brightness is required to explain the expected electromagnetic emission from secondary cascades of hadronic particles. The lack of  $\gamma$ -ray emission from the source is not fully consistent with this picture. The inconsistency may be explained if the high densities required for neutrino production in the source cause  $\gamma$  pair production of the high-energy photons (Zhang & Cheng 1997). Additionally, we performed follow-up observations of source #1 with X-Shooter and ATCA. The source is not detected in ATCA with strong constraints on the radio flux, and it is not detected by *Fermi*/*LAT*. Given the radio-quietness, the low  $\gamma$ -ray flux and the X-ray detection, the source is either not a blazar or a very faint/distant one. Our X-Shooter spectra has confirmed that source #1 is a type 1 Seyfert galaxy. ATCA follow-up of sources #2 and #3 show possible radio counterparts near the X-ray position. However, neither of them has been detected by *Fermi*/*LAT* and they are not in any catalogue. We therefore conclude that there is no blazar counterpart and no other obvious high-energy source counterparts as such, and its likely astrophysical origin remains a mystery. The neutrino localisation region was serendipitously located near the highest sensitivity location of the field-of-view of *Swift*/*BAT*. This constrains and rules out a bright GRB at the time and location of the neutrino. For future IceCube events at high signalness (high probability of being astrophysical in origin), a more rapid multiwavelength response with quasi-simultaneous data will help greatly in identifying the sources of high-energy neutrino alerts.



## ACKNOWLEDGEMENTS

We thank the anonymous referee for useful comments that have improved the manuscript. We thank R. Ciardullo for useful discussions and feedback on the draft. F. K. was supported as an Eberly Research Fellow by the Eberly College of Science at the Pennsylvania State University. P. A. E. acknowledges UKSA support. P. M. acknowledges support from the Eberly Foundation. M. S. is supported by NSF awards PHY-1914579 and PHY-1913607. We thank J.E. Davis for the development of the `slxfig` module that has been used to prepare the figures in this work. This research has made use of a collection of ISIS scripts provided by the Dr. Karl Remeis-Observatory, Bamberg, Germany at <http://www.sternwarte.uni-erlangen.de/isis/>. This research has made use of the NASA/IPAC Infrared Science Archive, which is funded by the National Aeronautics and Space Administration and operated by the California Institute of Technology. This publication makes use of data products from the Two Micron All Sky Survey, which is a joint project of the University of Massachusetts and the Infrared Processing and Analysis Center/California Institute of Technology, funded by the National Aeronautics and Space Administration and the National Science Foundation.

## REFERENCES

- Aartsen M., et al., 2013, *Science*, 342, 1242856
- Aartsen M. G., et al., 2017a, *Astroparticle Physics*, 92, 30
- Aartsen M. G., et al., 2017b, *ApJ*, 835, 45
- Aartsen M. G., et al., 2017c, *ApJ*, 843, 112
- Ayala Solares H. A., et al., 2019, *Astroparticle Physics*
- Barthelmy S. D., Butterworth P., Cline T. L., Gehrels N., Fishman G. J., Kouveliotou C., Meegan C. A., 1995, *Ap&SS*, 231, 235
- Barthelmy S. D., et al., 2005, *Space Science Reviews*, 120, 143
- Bechtol K., Ahlers M., Di Mauro M., Ajello M., Vandenbroucke J., 2017, *ApJ*, 836, 47
- Begelman M. C., Rudak B., Sikora M., 1990, *ApJ*, 362, 38
- Berezinskii V. S., Ginzburg V. L., 1981, *MNRAS*, 194, 3
- Beringer J., et al., 2012, *Phys. Rev. D*, 86, 010001
- Biermann P. L., Strittmatter P. A., 1987, *ApJ*, 322, 643
- Blandford R. D., 2000, *Physica Scripta Volume T*, 85, 191
- Boller T., Freyberg M. J., Trümper J., Haberl F., Voges W., Nandra K., 2016, *A&A*, 588, A103
- Buson S., Garrappa S., 2019, GRB Coordinates Network, 24040, 1
- Cardelli J. A., Clayton G. C., Mathis J. S., 1989, *ApJ*, 345, 245
- Cash W., 1979, *ApJ*, 228, 939
- Dermer C. D., Murase K., Inoue Y., 2014, *JHEAp*, 3-4, 29
- Eichler D., 1979, *ApJ*, 232, 106
- Evans P. A., et al., 2019, arXiv:1911.11710, pp 1–6
- Flesch E. W., 2017, *VizieR Online Data Catalog*, 7280
- GCN/AMON NOTICE IceCube-190331A 2017, IceCube-190331A, [https://gcn.gsfc.nasa.gov/notices\\_amon/15947448\\_132379.amon](https://gcn.gsfc.nasa.gov/notices_amon/15947448_132379.amon)
- Goldoni P., Royer F., François P., Horrobin M., Blanc G., Vernet J., Modigliani A., Larsen J., 2006, in *Society of Photo-Optical Instrumentation Engineers (SPIE) Conference Series*. p. 62692K, doi:10.1117/12.669986
- HI4PI Collaboration et al., 2016a, *A&A*, 594, A116
- HI4PI Collaboration Ben Bekhti N., Flöer L., Keller R., Kerp J., Lenz D., 2016b, *A&A*, 594, A116
- Haack C., Wiebusch C., 2017, *PoS, ICRC2017*, 1005
- Harrison F. A., et al., 2013, *ApJ*, 770, 103
- Hillas A. M., 1984, *ARA&A*, 22, 425
- Hooper D., Linden T., Vieregg A., 2019, *J. Cosmology Astropart. Phys.*, 2019, 012
- Houck J. C., Denicola L. A., 2000, in Manset N., Veillet C., Crabtree D., eds, *Astronomical Society of the Pacific Conference Series Vol. 216, Astronomical Data Analysis Software and Systems IX, ASP Conference Proceedings*, edited by Nadine Manset, Christian Veillet, and Dennis Crabtree. Astronomical Society of the Pacific. p. 591
- Huarte-Espinosa M., Frank A., Balick B., Blackman E. G., De Marco O., Kastner J. H., Sahai R., 2012, *MNRAS*, 424, 2055
- Ice Cube Collaboration I., 2019, *The Astronomer's Telegram*, 12616, 1
- IceCube Collaboration 2014, *Phys. Rev. Lett.*, 113, 101101
- IceCube Collaboration, Fermi-LAT Collaboration et al. 2018, *Science*, 361, eaat1378
- Icecube Collaboration 2019, GRB Coordinates Network, 24039, 1
- Jiménez-Bailón E., Chavushyan V., Scharfel N., Santos-Lleó M., Huerta E. M., Krongold Y., 2012, *AJ*, 143, 64
- Kadler M., et al., 2016, *Nature Physics*, 12, 807
- Keivani A., Murase K., Petropoulou M., Fox D. B., et al., 2018, *ApJ*, 864, 84
- Keivani A., Santander M., Kennea J. A., Evans P. A., Fox D. B., Krauss F., 2019, GRB Coordinates Network, 24094, 1
- Kelner S. R., Aharonian F. A., Bugayov V. V., 2006, *Phys. Rev. D*, 74, 034018
- Kopper C., Blaufuss E., 2017, GRB Coordinates Network, Circular Service, No., 21916
- Kraft R. P., Burrows D. N., Nousek J. A., 1991, *ApJ*, 374, 344
- Krauß F., et al., 2014, *A&A*, 566, L7
- Krauß F., et al., 2018, *A&A*, 620, A174
- Mannheim K., 1993, *A&A*, 269, 67
- Mannheim K., 1995, *Astroparticle Physics*, 3, 295
- Mannheim K., Biermann P. L., Kruells W. M., 1991, *A&A*, 251, 723
- McMullin J. P., Waters B., Schiebel D., Young W., Golap K., 2007, in Shaw R. A., Hill F., Bell D. J., eds, *Astronomical Society of the Pacific Conference Series Vol. 376, Astronomical Data Analysis Software and Systems XVI*. p. 127
- Modigliani A., et al., 2010, in *Observatory Operations: Strategies, Processes, and Systems III*. p. 773728, doi:10.1117/12.857211
- Murase K., Ioka K., 2013, *Phys. Rev. Lett.*, 111, 121102
- Murase K., Waxman E., 2016, *Phys. Rev. D*, 94, 103006
- Murase K., Ioka K., Nagataki S., Nakamura T., 2006, *ApJL*, 651, L5
- Murase K., Ahlers M., Lacki B. C., 2013, *Phys. Rev. D*, 88, 121301
- Murase K., Inoue Y., Dermer C. D., 2014, *Phys. Rev.*, D90, 023007
- Murase K., Kimura S. S., Meszaros P., 2019, arXiv:1904.04226, pp 1–10
- Norman C. A., Melrose D. B., Achterberg A., 1995, *ApJ*, 454, 60
- Padovani P., Resconi E., 2014, *MNRAS*, 443, 474
- Roming P. W. A., et al., 2005, *Space Sci. Rev.*, 120, 95
- Senno N., Mészáros P., Murase K., Baerwald P., Rees M. J., 2015, *ApJ*, 806, 24
- Senno N., Murase K., Mészáros P., 2016, *Phys. Rev. D*, 93, 083003
- Skrutskie M. F., et al., 2006, *AJ*, 131, 1163
- Smette, A. et al., 2015, *A&A*, 576, A77
- Stecker F. W., 2013, *Phys. Rev. D*, 88, 047301
- Stecker F. W., Done C., Salamon M. H., Sommers P., 1991, *Phys. Rev. Lett.*, 66, 2697
- Tamborra I., Ando S., 2016, *Phys. Rev. D*, 93, 053010
- Tavecchio F., Ghisellini G., 2015, *MNRAS*, 451, 1502
- Verner D. A., Ferland G. J., Korista K. T., Yakovlev D. G., 1996, *ApJ*, 465, 487

- Vernet J., et al., 2011, *A&A* , 536, A105  
Waxman E., Bahcall J., 1997, *Phys. Rev. Lett.*, 78, 2292  
White N. E., Giommi P., Angelini L., 1994, in *The WGA Catalog of ROSAT Point Sources*. p. 41.11  
Wilms J., Allen A., McCray R., 2000, *ApJ* , 542, 914  
Wright E. L., et al., 2010, *AJ* , 140, 1868  
Yuan C., Murase K., Mészáros P., 2020, *ApJ* , 890, 25  
Zhang L., Cheng K. S., 1997, *ApJ* , 475, 534

#### DATA AVAILABILITY

Data from *Swift* and *NuSTAR* data are publicly available on HEASARC (<https://heasarc.gsfc.nasa.gov/>). 2MASS and WISE data are available publicly at <https://irsa.ipac.caltech.edu/frontpage/>. Raw ATCA data are available at <https://atoa.atnf.csiro.au/query.jsp>. X-Shooter data are available on request.

This paper has been typeset from a  $\text{T}_{\text{E}}\text{X}/\text{L}^{\text{A}}\text{T}_{\text{E}}\text{X}$  file prepared by the author.